Bubble clouds and their transport within the surf zone as measured with a distributed array of upward-looking sonars

Peter H. Dahl

Applied Physics Laboratory, College of Ocean and Fishery Sciences,

1013 N.E. 40th Street, Seattle, Washington 98105-6698

(September 20, 2000)

Accepted August 28, 2000

Abstract

A collaborative, multi-institute experiment called the Scripps Pier Experiment was conducted in the vicinity of the Scripps pier in La Jolla, California, in March 1997 to study the fate of bubbles in the surf zone and the effects of these bubbles on acoustic propagation. This paper discusses data gathered by the Applied Physics Laboratory, University of Washington, using a set of four upward-looking sonars (frequency 240 kHz), which simultaneously measured vertical profiles of acoustic volume scattering from bubbles at four locations. The transport of bubbles via rip currents emerged as an important, though episodic and localized, feature of the acoustic environment in the surf zone. Images of volumetric backscattering strength vs time and depth reveal the episodic events (of increased scattering level) lasting between 5 and 10 min caused by the passage of bubble clouds over the sonar. Time lags for the onset of increased scattering at the four locations are consistent with a seaward velocity of the bubble clouds of order 10 cm/s, and the length scales of these bubble clouds in the seaward direction are inferred to be in the range 50 to 100 m. The influence of the incoming surface wave field is also discussed.

43.30Ft, 43.30.Pc

REPORT DOCUMENTATION PAGE

Form Approved
OMB No. 0704-0188

1. AGENCY USE ONLY (Leave Blank)	2. REPORT DATE	3. REPORT TYPE AND DATES COVERED
	20 September 2000	Final (2/1/99 - 3/31/00)

4. TITLE AND SUBTITLE
Bubble clouds and their transport within the surf zone as measured with a distributed array of upward-looking sonars

5. FUNDING NUMBERS
N00014-99-1-0322

6. AUTHOR(S)
Peter H. Dahl

7. PERFORMING ORGANIZATION NAME(S) AND ADDRESS(ES)
Applied Physics Laboratory
University of Washington
1013 NE 40th St.
Seattle, WA 98105-6698

8. PERFORMING ORGANIZATION REPORT NUMBER

9. SPONSORING/MONITORING AGENCY NAME(S) AND ADDRESS(ES)
Office of Naval Research
800 N. Quincy St.
Arlington, VA 22217-5660
Attn: Dr. Edward A. Estalote, Code 321OA

10. SPONSORING/MONITORING AGENCY REPORT NUMBER

11. SUPPLEMENTARY NOTES

Report was accepted on August 28, 2000, for publication in the Journal of the Acoustic Society of America.

12a. DISTRIBUTION/AVAILABILITY STATEMENT

Approved for public release

12b. DISTRIBUTION CODE

13. ABSTRACT (Maximum 200 words)

A collaborative, multi-institute experiment called the Scripps Pier Experiment was conducted in the vicinity of the Scripps pier in La Jolla, CA, in March 1997 to study the fate of bubbles in the surf zone and the effects of these bubbles on acoustic propagation. This paper discussed data gathered by the Applied Physics Laboratory, University of Washington, using a set of four upward-looking sonars (frequency 240 kHz), which simultaneously measured vertical profiles of acoustic volume scattering from bubbles at four locations. The transport of bubbles via rip currents emerged as an important feature of the acoustic environment. Images of volumetric backscattering strength vs time and depth reveal episodic events lasting between 5 and 10 minutes. The influence of the incoming wave field is also discussed

14. SUBJECT TERMS

acoustic scattering from bubbles, surf zone, rip currents

15. NUMBER OF PAGES
20

16. PRICE CODE

17. SECURITY CLASSIFICATION OF REPORT	18. SECURITY CLASSIFICATION OF THIS PAGE	19. SECURITY CLASSIFICATION OF ABSTRACT	20. LIMITATION OF ABSTRACT
Unclassified	Unclassified	Unclassified	UL

Applied Physics Laboratory
College of Ocean and Fishery Sciences, University of Washington

2 November 2000
Serial 5C5377

To: Dr. Edward A. Estalote
Office of Naval Research, Code 321OA
Ballston Centre Tower One
800 N. Quincy St.
Arlington, VA 22217-5660

From: Peter H. Dahl, Principal Investigator

Subj: ONR Grant N00014-99-1-0322, "Analysis of Scripps Pier Data"

Encl: (1) "Bubble clouds and their transport within the surf zone as measured with a distributed array of upward-looking sonars," including Report Documentation Page (SF-298) (3 copies, with copy of DTIC 50 card)

Enclosed please find three copies of the report on analysis of data from the Scripps Pier Experiment of March 1997. This document constitutes the Final Technical Report of research on the subject grant.

Peter H. Dahl

cc: Administrative Grants Officer, ONRRO Seattle (C.C. Everley) (SF-298 only, with copy of DTIC 50 card)
Naval Research Laboratory Code 5227
Defense Technical Information Center (2 copies, with DTIC 50 card)
Grant & Contract Services, University of Washington (S. Simmons) (w/o enclosure)
Grant & Contract Administrator, APL-UW (M. McCrory) (w/o enclosure)

INTRODUCTION

The surf zone is an extremely challenging environment for the operation of sonars. Although its shallowness means that sound transmission through the surf zone must invariably include interaction with its surface and bottom boundaries, the defining acoustic characteristic of the surf zone is the high concentration of bubbles. The process of bubble generation in the surf zone has been studied by Deane,[1,2] whose focus has been on the sound produced by bubbles associated with individual breaking waves. Deane showed through the analysis of photographic images taken within the active wave breaking region of the surf zone (or breaker zone) that air entrainment by shallow water breaking wavecrests forms bubbles whose radii a span the range $O(10)$ μm to $O(10)$ mm, and that these bubbles can be organized into clouds which commonly extend a meter into the water column within the breaker zone (or about half the total depth).

Immediately seaward of the breaker zone within which bubble generation occurs, rip currents, which are narrow strong return flows directed seaward,[3,4] can play a important role in determining the fate of bubbles in the surf zone. The Scripps Pier Experiment was conducted during the first two weeks of March 1997, off the Scripps pier in La Jolla, California. Its primary objective was to measure properties of bubbles within the outer region of the surf zone, such as bubble concentration and size distribution, the spatial and temporal scales of organized bubble clouds, and the transport and diffusion of bubbles as mediated by rip currents. To accomplish this objective, instruments for measuring bubbles, ambient noise, and surface waves were assembled by the Naval Research Laboratory at the Stennis Space Center (NRL-SSC), the Institute of Ocean Sciences (IOS), the Scripps Institute of Oceanography (SIO), and the Applied Physics Laboratory, University of Washington (APL-UW). These instruments were deployed 10 m off the north side of the Scripps pier, nominally 50 to 100 m seaward of the breaker zone, depending on tidal stage.

This paper discusses the measurements made by APL-UW during the Scripps Pier Experiment, using a distributed array of four upward-looking sonars, each called a SALMON

unit, for Shallow water Acoustic Lightweight MONitor. When combined into an array, these units simultaneously measured vertical profiles of acoustic volume scattering from bubbles at their respective locations within the measurement field. The experiment and measurement system are described further in Sec. I. In Sec. II we briefly discuss the topic of acoustic scattering from bubbles to make clear the nature of our measurements, the corrections applied in the initial data processing, and our notation. Also discussed in this section is a new way of quantifying the range of bubble radii that contribute to backscattering as function of acoustic frequency. Observations are presented in Sec. III. These are in the form of images of volumetric backscattering strength vs time and depth, which reveal the effects of seaward advection of large-scale bubble clouds by rip currents. Additionally, time averages of the data are presented, which yield estimates of the bubble concentration and the characteristic depth to which the bubbles have been dispersed during the course of their advection. A summary is given in Sec. IV.

I. EXPERIMENTAL MEASUREMENT SYSTEM

Figure 1 shows three of the four SALMON units prior to their 10-day deployment in the surf zone off the Scripps pier. Each unit consists of a stout frame housing a transducer and instrument case containing transmitting and receiving electronics, a pressure wave gauge, and a tilt meter. The units were controlled from a base on the Scripps pier via underwater cables, and important system diagnostics, e.g., tilt, could be ascertained remotely. The units were hand carried and lowered into the water for final positioning by divers from NRL-SSC and operated on demand throughout the 10-day deployment in the punishing underwater environment of the surf zone.

The four transducers transmitted simultaneously (with a source level of 179 dB re μPa at 1 m) at 0.5-s intervals a rectangular pulses of width of 0.1 ms and center frequency 240 kHz, giving a vertical resolution of approximately 8 cm. The one-way half-power beamwidth of all four transducers was 6°. The face of each transducer was placed 0.67 m above the seabed,

and data recording started after a time delay equivalent to a range of 0.7 m to ensure that measurements were made in the transducer's far field ($\sim$ 0.5 m). Data from the pressure gauges were recorded simultaneously along with the acoustic data but at 0.25-s intervals. These pressure measurements were converted to sea surface elevation above each sensor unit, assuming the measured pressure field was hydrostatic. In addition to wave height and wave spectral information, the pressure data were used to establish the location of the air/sea interface during periods of severe acoustic attenuation from bubbles.

The NRL-SSC delta frame,[5] an equilateral triangle with sides of approximately 10 m, established the primary locus of measurement activity. The delta frame was placed 10 m north of the Scripps pier between pier pilings 33 and 34. Figure 2 shows the location of the delta frame with respect to the Scripps pier and the four SALMON units. Two of the four units (units 1 and 2) were located along a line parallel to the anticipated seaward flow of bubbles, and two units (units 3 and 4) were offset on either side of this line. This layout was intended to maximize the ability to measure the larger spatial scales of a bubble field as it advected over the delta frame.

More information concerning the delta frame is given by Caruthers *et al.*,[5] who discuss the results of the multi-frequency sound propagation and attenuation measurements made by NRL-SSC during the Scripps Pier Experiment. Also, Vagle *et al.*,[6] Farmer *et al.*,[7] and Terrill and Melville[8] discuss measurements made by IOS and SIO which included horizontal-looking sonars directed shoreward from the Scripps pier and instruments for measuring the bubble size distribution in the breaker zone. These works, along with this paper, constitute a developing set of archival works covering the 1997 Scripps Pier Experiment. The observations of bubbles presented in this paper complement those presented in Refs. 5–8 insofar as our measurements reveal information on the vertical distribution of bubbles, as measured at four locations, and the seaward flow speeds of organized bubble clouds, as inferred from the time delay between the arrival of the increased scattering associated with these bubble clouds at each sensor location.

II. ACOUSTIC SCATTERING FROM BUBBLES

Our measurements of bubbles are in the form of the backscattering cross section per unit solid angle, or s_v [m^{-1}], which is defined by the integral

$$s_v = \int \sigma_{bs}(a) N(a) da, \tag{1}$$

where $\sigma_{bs}(a)$ is the backscattering cross section of a single bubble, and $N(a)$ is the bubble size distribution function giving the number of bubbles per cubic meter per unit radius for radii between a and $a + da$. For $\sigma_{bs}(a)$ we use (e.g., c.f. Ref. 9)

$$\sigma_{bs}(a) = \frac{a^2}{[(f_R/f)^2 - 1]^2 + \delta^2} \tag{2}$$

which is valid for $ka \ll 1$, where k is the acoustic wavenumber; δ is the total damping coefficient, f is the frequency, and f_R is the resonant frequency. The resonant frequency is related to the bubble radius and depth z by $f_R = 3.25\sqrt{1 + 0.1z}/a$, where all units are in MKS. We report the decibel equivalent, $S_v = 10 \log_{10} s_v$, in dB re m^{-1}. The sonar equation is used to compute initial estimates of s_v vs range from the sonar, which are then corrected for the effects of excess attenuation from bubbles. Knowledge of the bubble size distribution is required for this procedure, and thus we incorporate information about $N(a)$ derived from the multi-frequency attenuation measurements made during the Scripps Pier Experiment by Caruthers *et al.*[5] and Terrill and Melville.[8] Specifically, Caruthers *et al.* report estimates of $N(a)$ for bubbles with radii in the range 16 to 100 μm. Below is a good representation of all six $N(a)$ functions shown in their Figs. 10–15, expressed here as $n(a)$; $n(a)$ differs from $N(a)$ by a multiplicative constant scaling factor q, which can be set with either a known void fraction or s_v:

$$n(a) = 1, \quad 16\ \mu\text{m} \leq \text{a} \leq 40\ \mu\text{m} \tag{3a}$$

$$n(a) = (a/40\ \mu\text{m})^{-3.4}, \quad 40\ \mu\text{m} < \text{a} \leq 100\ \mu\text{m}. \tag{3b}$$

For small bubbles, we postulate that $n(a)$ behaves as

$$n(a) = (a/16\ \mu\text{m})^3, \quad \text{a} < 16\ \mu\text{m}. \tag{3c}$$

For large bubbles, we take the a^{-5} power law behavior reported by Terrill and Melville, giving

$$n(a) = (a/100\ \mu\text{m})^{-5}, \quad \text{a} > 100\ \mu\text{m}. \tag{3d}$$

The range of bubble radii a is such that $1\ \mu\text{m} \leq a \leq 200\ \mu\text{m}$. It is not surprising that the $N(a)$ associated with bubbles near the delta frame measurement area is quite different from the one that Deane estimated from photographic evaluation of nascent bubbles in the active breaker zone, e.g., as in Fig. 7 of Ref. 1. By the time bubbles have advected from the breaker zone where they are generated to the delta frame, they have existed for $O(10)$ min.

Corrections for bubble-mediated excess attenuation commence at a range of 1 m from the sonar. The value of S_v at that point, called S_{v_0}, is used for correcting S_v in the next range bin, and so on up to the sea surface, which produces a distinctive reflection. A new scaling factor q is computed at each of the range bins, which are separated by $dR = 3$ cm. For example, at the starting range, where no correction is applied,

$$q_1 = \frac{10^{S_{v_0}/10}}{\int_{1\mu\text{m}}^{200\mu\text{m}} \sigma_{bs}(a) n(a) da}. \tag{4}$$

Next, the bubble-mediated attenuation α_1 (in dB/m) that is applied to the uncorrected S'_{v_1} in the next range bin is given by

$$\alpha_1 = 4.34 q_1 \int_{1\mu\text{m}}^{200\mu\text{m}} \sigma_e(a) n(a) da, \tag{5}$$

where $\sigma_e(a)$ is the extinction cross section per unit volume and equals $(4\pi\delta/ka)\sigma_{bs}$. We proceed to convert uncorrected values S'_{v_j} to corrected values S_{v_j} via

$$S_{v_j} = S'_{v_j} + 2dR \sum_{j=1}^{N} \alpha_j. \tag{6}$$

Note that there are a few instances where the bubble concentration is sufficiently high as to nearly extinguish the sound pulse and prevent backscatter from the sea surface. Under these circumstances, the correction procedure, which is essentially a first-order multiple scattering

representation,[10] is no longer valid. The air/sea interface, however, can still be located using the pressure time series. Note that for strong, but otherwise measurable, backscatter, e.g., for $S_v = -25$ dB, α equals about 0.5 dB/m, which is comparable to direct measurements of attenuation made at 244 kHz by Caruthers *et al.*[5]

It is useful to evaluate how backscattering measurements made at 240 kHz respond to this bubble size distribution. For this we define the probability density function (PDF) $p(a_s)$ by recognizing that the positive quantities $\sigma_{bs}(a)$ and $n(a)$ can be combined into a PDF for the variable a_s. (On the basis of the Lebesgue decomposition theorem,[11] any non-negative function that integrates to unity can be identified as a PDF for some variable.) The variable a_s is defined as the radius of a bubble contributing to the backscatter at a specified acoustic frequency, where

$$p(a_s) = \frac{\sigma_{bs}(a_s)n(a_s)}{\int_{1\mu\text{m}}^{200\mu\text{m}} \sigma_{bs}(a)n(a)da}, \tag{7}$$

and the sample space over which a_s is defined is the same as the range for a (1–200 μm). Figure 3 shows the PDF corresponding to the $n(a)$ described above and a frequency of 240 kHz, along with one based on a frequency of 70 kHz; note the dominant effect of scattering by resonant-sized bubbles at the lower frequency. We shall call the expected value $E(a_s)$ the *scattering centroid*, or *sc*, and the square root of the variance $E(a_s - sc)^2$ the *scattering spread*, or δsc. With the above representation of $n(a)$, then $sc = 55$ μm and $\delta sc = 39$ μm at 240 kHz, and $sc = 53$ μm and $\delta sc = 15$ μm at 70 kHz. A good measure of the central tendency of volumetric backscattering from bubbles vis-à-vis bubble radius is to take a range $\pm$ δsc about *sc*. For example, at 240 kHz approximately 90% of the scattered intensity is due to bubbles with radii of 16 to 94 μm, while at 70 kHz this range narrows to 38 to 68 μm. Importantly, these *sc* and δsc values for 240 kHz are relatively insensitive to alternative representations of the behavior of $n(a)$ at the bubble radii of < 16 μm that we have postulated.

Finally, S_v is mapped to void fraction, defined as the ratio of the volume of air to the volume of the sample region. The mapping assumes a sonar frequency of 240 kHz plus the

$n(a)$ defined above for bubble radii between 1 and 200 μm, and is as follows:

$$\log_{10} \text{void fraction} = 0.1 S_v - 3.67. \tag{8}$$

Since $n(a)$ goes as a^{-5} for larger bubble radii, smaller bubbles are more important for determining void fraction (see Ref. 1 for further discussion on this point). This mapping produces a higher void fraction (by about a factor of 7) for a given S_v than the result given by Dahl and Jessup[12] for the same frequency, obtained in studies of ambient oceanic bubble populations. One expects this, however, since most studies of ambient oceanic bubble populations, e.g., those reported by Vagle and Farmer,[13] show $n(a)$ reaching a maximum in the vicinity of 20 μm.

III. OBSERVATIONS

Acoustic transmissions from the SALMON units were coordinated with measurement periods of the other instruments located on or near the delta frame to prevent interference. A synchronized measurement run lasted typically 5000 s, or 83 min and 20 s. In this paper, as in Ref. 5, we discuss results from measurement run 7, which began at 1426 PST on 8 March. As noted in Ref. 5, rip currents were more prevalent during periods of low tide, which produced active surf breaking and swash in the region nominally 100–150 m shoreward of the delta frame measurement area. A spring tide was in effect on 8 March, with the start of run 7 coinciding with the low water point and the beginning of the incoming tide. The mean water depth at unit 2 (as determined from the pressure data after time averaging to remove wave effects) at the start of run 7 was 4 m, which increased to 4.25 m over the next 80 min.

Figure 4 shows a surface wave height frequency spectrum from run 7, as determined by the pressure data from unit 3. The rms wave height is about 0.3 m, and there is a broad peak in the vicinity of 0.1 Hz. Interestingly, there is also a significant peak near 0.06 Hz, which is possibly associated, through nonlinear interaction,[14] with the peak near 0.18 Hz.

Given the mean water depth of 4 m, the peak at 0.1 Hz corresponds, via finite-depth linear theory, to a wavelength of 61 m. However, the time series of surface elevation show nonlinear effects such as an extended duration of the trough phase compared to that of the peak phase. Using the dispersion relation for finite-depth, nonlinear Stokes waves[15] and taking a typical wave amplitude to be 0.4 m puts the wavelength at 0.1 Hz closer to 63 m. (The influence of these nonlinear waves on the structure of bubble clouds is illustrated in Fig. 7.)

Figure 5 shows an 80-min display of S_v (with the above corrections for bubble attenuation applied) vs depth and time (representing 96% of run 7). The plots in Fig. 5 are arranged such that their order, from top to bottom, represents units 2-4-3-1, or increasing distance in the seaward direction (see Fig. 2). The sea surface is represented on each plot by the brown color indicative of intense backscatter (essentially reflection) from the air/sea interface, and the vertical depth scale on each plot is referenced to a nominal mean still water level. Although rip currents do carry a sediment load which increases optical turbidity (see, e.g., Smith and Largier[16]), we shall assume, based on the huge scattering advantage of bubbles over that of suspended particulates, that scattering from within the water column is associated primarily with entrained bubbles. As remarked earlier, our procedure for correcting bubble attenuation is not applicable when bubbles are in such high concentration that the sound pulse is nearly extinguished owing to bubble scattering and absorption. This condition is shown in the top plot between minutes 14 and 17 and in the third-from-top plot between minutes 15 and 17.

Letters A–E, shown only in the uppermost plot, identify five sustained periods of increased bubble scattering, which we have classified as episodic events and interpret as the passage of organized, large-scale, bubble clouds. This classification is somewhat arbitrary; e.g., events C and D have early and late phases, each of which could constitute a separate event. However, we choose to define an event as the existence of a well-defined scattering front caused by a rapid increase in scattering level that (1) first appears in the data from unit 2 and (2) then in the data from the other three units located seaward of unit 2, with approximately the same scattering strength and duration but with increasing delay with

increasing seaward location of the sensor unit. The one exception is event B, in which the front arrives at unit 3 about 30 s before it arrives at unit 4, just shoreward of unit 3. These same five events can be identified in Fig. 6 of Caruthers *et al.*,[5] which shows five periods of sustained high bubble attenuation (including the early and late phases of events C and D). Based on the time delay between the arrival of these fronts at the three units located seaward of unit 2, we estimate the seaward advection speed V_{df} at the delta frame site to be 7, 19, 7, 17, and 20 cm/s for events A–E, respectively.

The delay effect is best viewed with a less compressed time scale such as that in Fig. 6, which shows a 25-min subset of the data shown in Fig. 5 including the fronts associated with events C and D. The small white triangles in the top and bottom plots each point to a smaller scattering feature about 45 s in duration seen only on inner unit 2 and, 55 s later, on outer unit 1. We postulate that this scattering feature originates from the same discrete bubble cloud, and the inferred seaward velocity of this bubble cloud is 0.25 m/s. If we invoke Taylor's frozen turbulence hypothesis, the 45 s duration implies that the cloud's extent, or outer scale, in the seaward direction L_S (parallel to the pier) is $\sim$ 11 m. The fact that the cloud is detected only by units 2 and 1 implies that the cloud's extent in the longshore direction L_L (perpendicular to the pier) is < 12 m. Using similar arguments, we find that the larger organized bubble clouds associated with scattering events A–E all have $L_L > 12$ m, based on the fact that these events eventually produce a simultaneous scattering response on all four units. Their seaward extents can also be inferred by the scattering duration, which ranges from about 5 to 10 min, combined with their inferred velocities; these results put L_S in the range of 50 to 100 m. Thus, area coverage of these organized bubble clouds is in the range of 500 to 1000 m^2. Finally, there are itermittent periods of temporal variation in S_v that appear to be related to the dominant frequency of the surface waves. (For example, as depicted in the bottom plot of Fig. 6 near the label C.) Mechanisms for this variation may be, in part, similar to those discussed by Dahl and Plant.[17] This will be investigated in more detail in future work.

Figure 7 shows 65 s of data from inner unit 2 (top plot) and outer unit 1 (middle plot) corresponding to the passage of the discrete bubble cloud seen only by these two units and identified by the white triangles in Fig. 6. The time scale for the middle plot has been shifted by 55 s in order to compare the data. The bold white line on the top and middle plots shows the location of the air/sea interface as determined from the pressure records. At both times and locations, the cloud's bottom contour with respect to a fixed reference frame is governed by water column displacements associated with the dynamics of surface waves. The surface wave field above the outer sensor (and 55 s later) provides a particularly nice illustration of nonlinearities in the surface waves. The dashed line in the middle plot tracing a portion of the cloud's bottom contour at the location of unit 1 is simulated vertical displacement associated with a finite-depth Stokes wave. The parameters for this wave are wave period 11 s, wave amplitude a 0.35 m, and depth 4.4 m, which corresponds to a wave number of 0.0869 radians/m, or a wavelength of 72 m. (Note that the wave amplitude is such that $2a$ corresponds to the peak-to-trough height of the Stokes wave.) The equation for vertical displacement giving the dashed line is derived from Whitham's[15] equation for the velocity potential of a finite-depth Stokes wave, carried out to $O(a^2)$.

Finally, the bottom plot of Fig. 7 shows the depth-averaged s_v (in dB) of the bubble cloud measured at each location. This processing largely removes differences due to the variation in the surface wave field, and the two depth-averaged time series now appear quite similar, lending further credence to our assertion that these are indeed the same bubbles. Again, assuming that a Taylor's frozen turbulence hypothesis applies, and using an advection speed of 0.25 m/s, we see that coherent structure on scales of order 1 m in the seaward dimension is preserved in the course of advection over the delta frame site.

Figure 8 shows a time series of void fraction as measured by the sonar located on SALMON unit 2. The void fraction estimate was calculated from Eq. (8), using $S_v = 10\log_{10}\langle s_v\rangle_z$, where in this case $\langle s_v\rangle_z$ is a depth average over a 0.25-m-thick layer centered at 1 m (thick gray line) and 2 m (thick dashed line) below the time-varying sea surface (with sea surface elevation determined by the pressure data). Upon taking the depth average, the

result was then time averaged over a 30 s window equivalent to 60 sonar pulses. Letters A–E corresponding to the five primary bubble-scattering events first depicted in Fig. 5 are also shown on this figure. A characteristic time scale for the events, defined as a sustained high void fraction that exceeds 10^{-7}, ranges between 5 and 10 min. Alternatively, event B is particularly suited to using an exponential decay law to describe the decay in void fraction after its initial sharp onset. Here, the time constant of the exponential is 4 min, and the decay law is shown by the dotted-dashed line.

The void fraction within the layer centered at 1 m is, for the most part, greater than or equal to that found in the layer centered at 2 m. A notable exception is the start of event B, where as remarked earlier the signal in the upper region of the water column is reduced owing to bubble attenuation . Also, the smaller bubble cloud seen near the surface and discussed in Fig. 7 produces an abrupt jump in void fraction seen only in the 1-m data shortly after min 31. Thus this cloud would not have been detected by instruments mounted on the delta frame.

To evaluate further the dependence of void fraction on depth, the void fraction is averaged over a time window corresponding (approximately) to the uninterrupted time span during which the the void fraction exceeds 10^{-7} for each event. Figure 9 shows the time-averaged void fraction vs depth beneath the time-varying sea surface for the five events (plots labeled A–E, along with their advection speeds) and their overall average (plot labeled AVG along with the average advection speed). The event time averages are computed for each sensor separately, with data from each sensor shown by the thick, colored lines. The overall average (thick, black line in the lower right plot) corresponds to an average over all four sensor units and all five events. A background time-averaged void fraction vs depth for each unit is also shown (thin, dashed colored lines), along with the average over all four units (thin, dashed black line) in the plot at the lower right. The background estimates are derived by averaging over times (such as in the vicinity of minute 30 in Fig. 5) between high-scattering events.

With exception of event A, where the data from unit 4 (green line) and unit 2 (red line) are significantly lower and higher, respectively, than data from the other two units, the data

from the four units display a central tendency in both level and depth scale. This tendency is illustrated in the overall average shown in the lower right plot. The average background void fraction during run 7 is about $10^{-7.5}$, which itself is acoustically significant, and the void fraction increases by roughly an order of magnitude owing to the influx of bubbles advected by a rip current. The dashed red lines plotted over the average results are simple representations based an exponential reduction in void fraction with distance z beneath the time-varying surface elevation. This representation is

$$\beta(z) = \beta_0 e^{-z/L_z}, \tag{9}$$

where β is the average void fraction, L_z is the exponential depth scale, which is 2.3 m and applies to both background and events, and β_0 is the average void fraction just below the air–sea interface, which is $10^{-7.2}$ for the background and 10^{-6} for the events. The dashed horizontal line at 10 cm in the lower right plot marks the point where pulse resolution limits our ability to reliably distinguish between volume scattering from entrained bubbles and surface scattering from the air–sea interface. Thus, averaged data above this line are of questionable value. We would expect reality to lie between the averaged data and the exponential decay law.

Finally, we can make a crude estimate of the time T over which bubbles have undergone advection, starting from their generation within the breaker zone and ending at the delta frame measurement site, by projecting the estimated rip current speeds back toward the breaker zone. For this we shall assume that most of the rip current field between the breaker zone and the delta frame is confined within a fixed-width channel and that the current undergoes minimal lateral expansion in the longshore dimension. This inner part of the rip current field is called the neck. At a point farther seaward, the current does expand laterally, becoming more eddylike, and this outer part of the current is called the rip head.[18] If we assume, furthermore, that the flow is uniform in depth at least within the neck region,[19,20] then by mass conservation the speed of the seaward current increases with distance X from the delta frame in the direction toward the breaker zone, and goes as

$V(X) = \frac{4V_{df}}{4 - X\tan(1.2°)}$, where V_{df} is the current speed estimated at the delta frame, 1.2° is the nominal bottom slope,[6] and 4 m is the water depth at sensor unit 2.

We take the nominal distance from the delta frame to the breaker zone to be 75 m, giving $T \approx 300$ s when V_{df} is 20 cm/s and $T \approx 870$ s when V_{df} is 7 cm/s. Next, we estimate the magnitude of the average vertical eddy diffusivity, k_v, based on bubbles mixing to depth L_z over a time scale T, using $k_v \sim \frac{L_z^2}{2T}$. This puts k_v in the range 0.003 to 0.009 m^2/s, and varying linearly with V_{df} within this range. These magnitude estimates for k_v are reasonably consistent with more precisely modeled estimates of k_v recently computed by Vagle *et al.*[6] based on a turbulent boundary layer model. We expect to carry out more detailed comparisons between the depth-dependent void fraction estimates presented here and the model for bubble diffusion in the surf zone discussed in Ref. 6.

IV. SUMMARY

Bubble clouds within the outer region of the surf zone have been studied using a distributed array of four upward-looking sonars as part of the 1997 Scripps Pier Experiment involving several organizations. The bubble clouds were created in the inner, or breaker zone, region of the surf zone by shoaling waves, and the bubbles reached the measurement site through the process of seaward advection by rip currents. This study demonstrates how the seaward transport of bubbles via rip currents can dramatically alter the acoustic environment in the outer region of the surf zone, when this outer region is fed by rip currents which are themselves both episodic and localized.

The sonar measurements were in the form of volumetric backscattering strength S_v (in dB) vs depth and time and were made at an acoustic frequency of 240 kHz. A function, proportional to the size distribution of bubbles transported by rip currents into the outer region of the surf zone, was defined. This function, $n(a)$, where a is bubble radius, represents an amalgamation of multifrequency bubble attenuation measurements, which were more sensitive to bubble radius, made by other members of the experimental collaboration. The

relation between $n(a)$ and frequency-dependent volumetric backscattering was also quantified by way of a PDF for the contribution to backscattering as a function of bubble radius at a specific acoustic frequency. At our frequency of 240 kHz, for example, bubble radii within the range 16 to 94 μm contributed 90% of the backscattered acoustic energy.

Depth-vs-time images of S_v revealed episodes of high scattering, called scattering events, associated with the passage of large-scale bubble clouds over the four measurement locations. Five of such events, each of duration $O(100)$ s, were identified in the 83 min of continuous measurements examined here. Based on a mapping between S_v and void fraction, which depends on $n(a)$, the average void fraction over the duration of these events was of $O(10^{-6})$, with a somewhat higher void fraction observed over periods lasting a few seconds. We emphasize that our void fraction estimates depend on a mapping between our observable, s_v, and the void fraction, based on the form for the bubble size distribution, $n(a)$, discussed in this paper. The speed of seaward advection of these bubble clouds was estimated from the delay between the arrival of the event's front at each of the four sonar locations. These speeds ranged from 7 to 20 cm/s, although the speed associated with a smaller scattering feature, seen only on two of the four sonar units, was estimated to be 25 cm/s.

The outer length scales in the seaward direction L_S of the bubble clouds associated with the high-scattering events were estimated from their duration time and the seaward advection speed. These calculations put L_S in the range of 50–100 m. In terms of the outer length scale in the longshore direction (L_L), this estimate was bounded by $L_L > 12$ m, since the events were eventually seen simultaneously at units 3 and 4, which were separated in the longshore direction by 12 m. A characteristic depth scale for the bubble clouds was estimated to be ~ 2.3 m. Using this value along with T, the time over which bubbles have undergone advection and vertical mixing, in the range 300–870 s, puts an estimate of the vertical eddy diffusivity k_v in the range 0.003–0.009 m^2/s.

The incoming wave field at the location of each unit was measured with a pressure gauge. The peak period of the frequency spectrum for the incoming wave field was close to 10 s, which translates to wavelengths of about 63 m according to finite-depth nonlinear

wave theory. The influence of this wave field was illustrated by modeling the time-varying interface between the organized bubble cloud and the surrounding water, which had a much lower concentration of bubbles, with a finite-depth Stokes wave.

ACKNOWLEDGMENTS

I wish to thank Robert Drever and Mike Welsh of APL-UW for critical engineering and field support in carrying out the Scripps Pier Experiment. I also thank Dr. Steve Stanic of NRL-SSC and the entire field crew and dive team from NRL-SSC for their assistance in the field. The discussions with Dr. Grant Deane of SIO are also much appreciated. This work was supported by the Office of Naval Research, Code 321 Ocean Acoustics, via contracts N00039-91-C-0072 and N00014-96-1-0325.

REFERENCES

[1] G. B. Deane, "Sound generation and air entrainment by breaking waves in the surf zone," J. Acoust. Soc. Am. **102**, 2671–2689 (1997).

[2] G. B. Deane, "Acoustic hot-spots and breaking wave noise in the surf zone," J. Acoust. Soc. Am. **105**, 3151–3167 (1999).

[3] D. R. Basco, "Surfzone current," Coastal Engineering **7**, 331–355 (1983).

[4] F. P. Shepard and D. L. Inman, "Nearshore water circulation related to bottom topography and wave refraction," Trans. Am. Geophys. Union **31**, 196–212 (1950).

[5] J. W. Caruthers, S. J. Stanic, P. A. Elmore, and R.R. Goodman, "Acoustic attenuation in very shallow water due to the presence of bubbles in rip currents," J. Acoust. Soc. Am. **106**, 617–625 (1999).

[6] S. Vagle, D. M. Farmer, and G. B. Deane, "Bubble transport in rip currents," submitted to *J. Geophys. Res.*, 2000.

[7] D. M. Farmer, G. B. Deane, and S. Vagle, "The influence of bubble clouds on acoustic propagation in the surf zone," submitted to *IEEE J. Oceanic Eng.*, 2000.

[8] E. J. Terrill and W. K. Melville, "Bubbles and surf zone oceanography," in Proc. 16th International Congress on Acoustics and the 135th Meeting of the Acoustical Society of America, pp. 703–704, 1998.

[9] C. S. Clay and H. Medwin, *Acoustical Oceanography* (Wiley, New York, 1977).

[10] A. Ishimaru, *Wave Propagation and Scattering in Random Media*, Vol. I (Academic, New York, 1978).

[11] K. L. Chung, *A Course in Probability Theory* (Academic Press, New York, 1974), see Theorem 1.3.2.

[12] P. H. Dahl and A. T. Jessup, "On bubble clouds produced by breaking waves: An event analysis of ocean acoustic measurements," J. Geophys. Res. **100**, 5007–5020 (1995).

[13] S. Vagle and D. M. Farmer, "A comparison of four methods for bubble size and void fraction measurements," IEEE J. Oceanic Eng. **23**, 211–222 (1998).

[14] S. Elgar and R. T. Guza, "Shoaling gravity waves: comparison between field observations, linear theory, and a nonlinear model," J. Fluid Mech. **158**, 47–70 (1985).

[15] G. B. Whitham, *Linear and Nonlinear Waves* (Wiley, New York, 1974).

[16] J. A. Smith and J. L. Largier, "Observations of nearshore circulation: Rip currents," J. Geophys. Res. **100**, 10,967–10,975 (1995).

[17] P. H. Dahl and W. J. Plant, "The variability of high-frequency acoustic backscatter from the region near the sea surface," *J. Acoust. Soc. Am.* **101**, 2596–2602 (1997).

[18] F. B. Shepard, *Submarine Geology* (Harper, New York, 1948).

[19] F. B. Shepard, with chapters by D. L. Inman and E.D. Goldbert, *Submarine Geology*, 2nd ed. (Harper & Row, New York, 1963).

[20] C. Miller, and A. Barcilon, "The dynamics of the littoral zone," Rev. Geophys. Space Phys. **14**, 81–91 (1976).

FIG. 1. Photograph of three of the four SALMON units made just prior to their deployment in surf zone waters off the Scripps pier.

FIG. 2. Plan view and grid of the experimental area showing the delta frame and locations of the four SALMON units, labeled 1–4. Bubbles entrained in the seaward flow of rip currents were first seen on unit 2, then 4, 3, and 1.

FIG. 3. Probability density function (PDF) for the variable a_s, defined as the radius of a bubble contributing to the backscatter for a set acoustic frequency. Two PDFs are shown, one for an acoustic frequency of 70 kHz and one for 240 kHz.

FIG. 4. Frequency spectrum corresponding to run 7, measured by the pressure sensor located at SALMON unit 3. For reference, the dotted line shows an slope of f^{-4}. A significant peak near 0.06 Hz and its third harmonic, 0.18 Hz, are identified by the markers.

FIG. 5. Depth-vs-time display of decibel equivalent of the backscattering cross section per unit volume, or S_v in dB. The 80 min duration represents 96% of run 7. The four plots are arranged such that their order, from top to bottom, represents data from SALMON units 2-4-3-1, or increasing distance in the seaward direction, as shown in Fig. 2. The sea surface is represented on each plot by the brown color. The depth axis is relative to a nominal mean still water level. The letters A–E, shown only in the top plot, identify five sustained periods of increased bubble scattering that are classified as events.

FIG. 6. Same as Fig. 5, but display of S_v starts 50 min after start of run 7, and duration is 25 min. Events C and D are now identified on the data displays of all four SALMON units. The two white triangles mark a scattering feature seen only on inner unit 2 and, 55 s later, on outer unit 1.

FIG. 7. Expanded view of depth-vs-time display of S_v showing 65 s of data from inner unit 2 (top plot) and outer unit 1 (middle plot). Note that the time scale for the middle plot is shifted by 55 s. The bold white lines in the top and middle plots represent the air/sea interface as determined from the pressure gauges located within each unit. The dashed line shown in the middle plot is simulated vertical displacement based on a finite-depth Stokes wave. The bottom plot shows depth-averaged s_v (expressed in dB) vs time, which removes the effect of a time-varying air/sea interface. The 1-m scale represents length in the seaward dimension based on an advection speed of 0.25 cm/s.

FIG. 8. Time series of void fraction measured by the sonar located on SALMON unit 2. The letters A–E correspond to the same events identified in Fig. 5. The dashed line corresponds to a 0.25-m-thick layer centered 2 m below the time-varying sea surface, and the solid, gray line corresponds to a 0.25-m-thick layer centered 1 m below the time-varying sea surface. The dotted line plotted over the data in the vicinity of event B is an exponential decay model with a time scale of 4 min.

FIG. 9. Time-averaged void fraction vs depth beneath the time-varying sea surface for the five events (plots labeled A–E, along with their advection speeds) and their overall average (plot labeled AVG along with the average advection speed). The event time-averages computed for each sensor separately are shown by the thick, colored lines. The overall average corresponds to an average over all four sensor units and all five events and is shown by the thick, black line in the lower right plot. A background time-averaged void fraction vs depth for each unit is also shown (thin, dashed colored lines), along with the average over all four units (thin, dashed black line in the lower right plot). Dotted horizontal line in the lower right plot corresponds to a depth of 10 cm and marks beginning of a region of ambiguity in surface resolution as determined by pulse length. The dotted lines plotted over the averaged data are simple exponential decay representations of the averaged data.

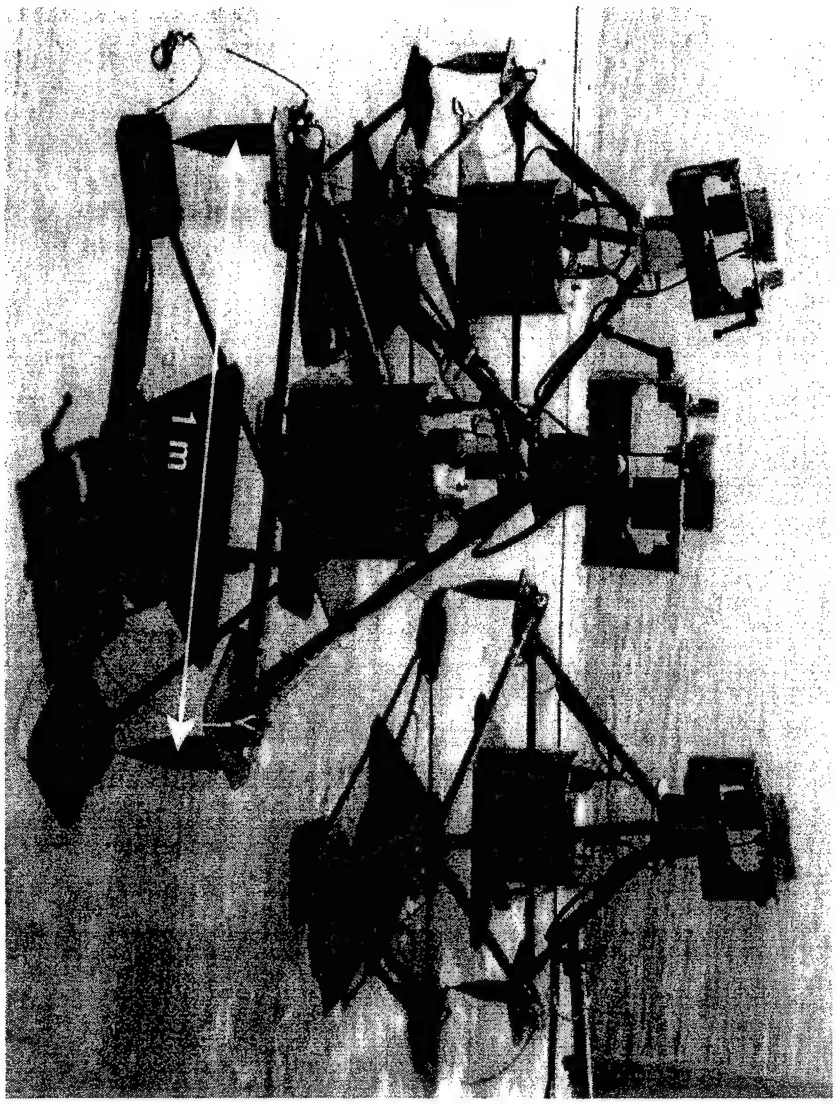

F1

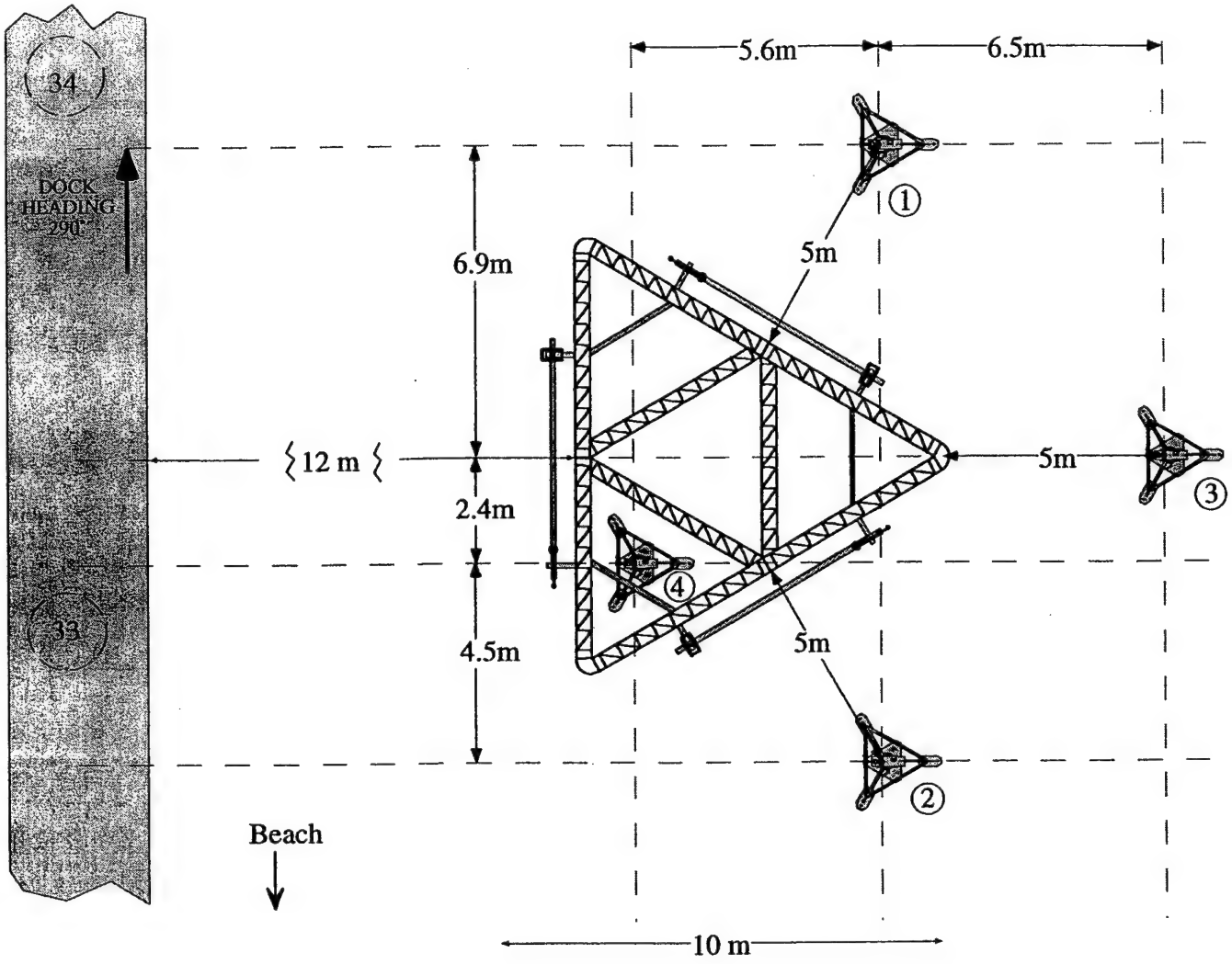
34
DOCK
HEADING
290°
33
5.6m
6.5m
6.9m
5m
12 m
5m
2.4m
4.5m
5m
1
2
3
4
Beach
10 m

F2

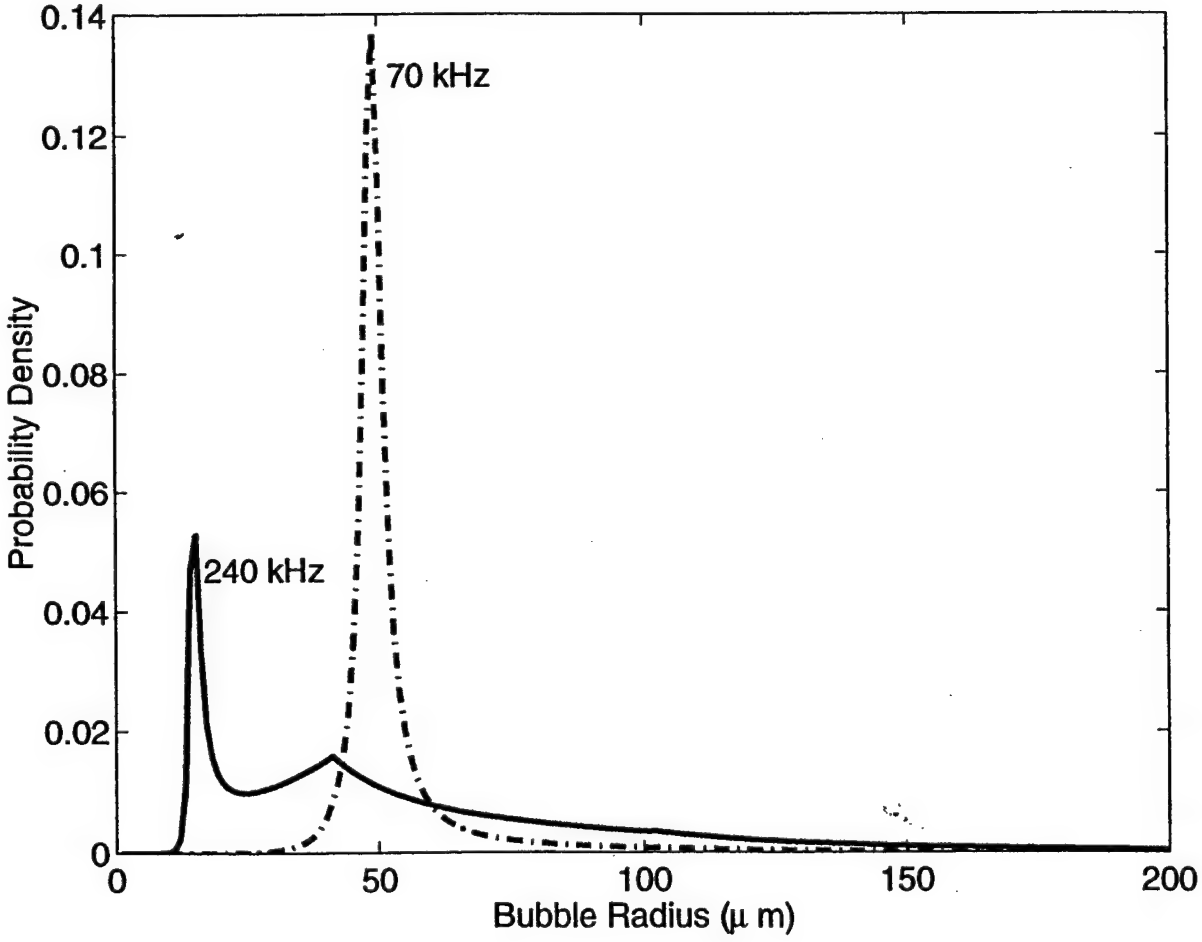
0.14
0.12
0.1
0.08
0.06
0.04
0.02
0
Probability Density
70 kHz
240 kHz
0
50
100
150
200
Bubble Radius (μ m)

F3

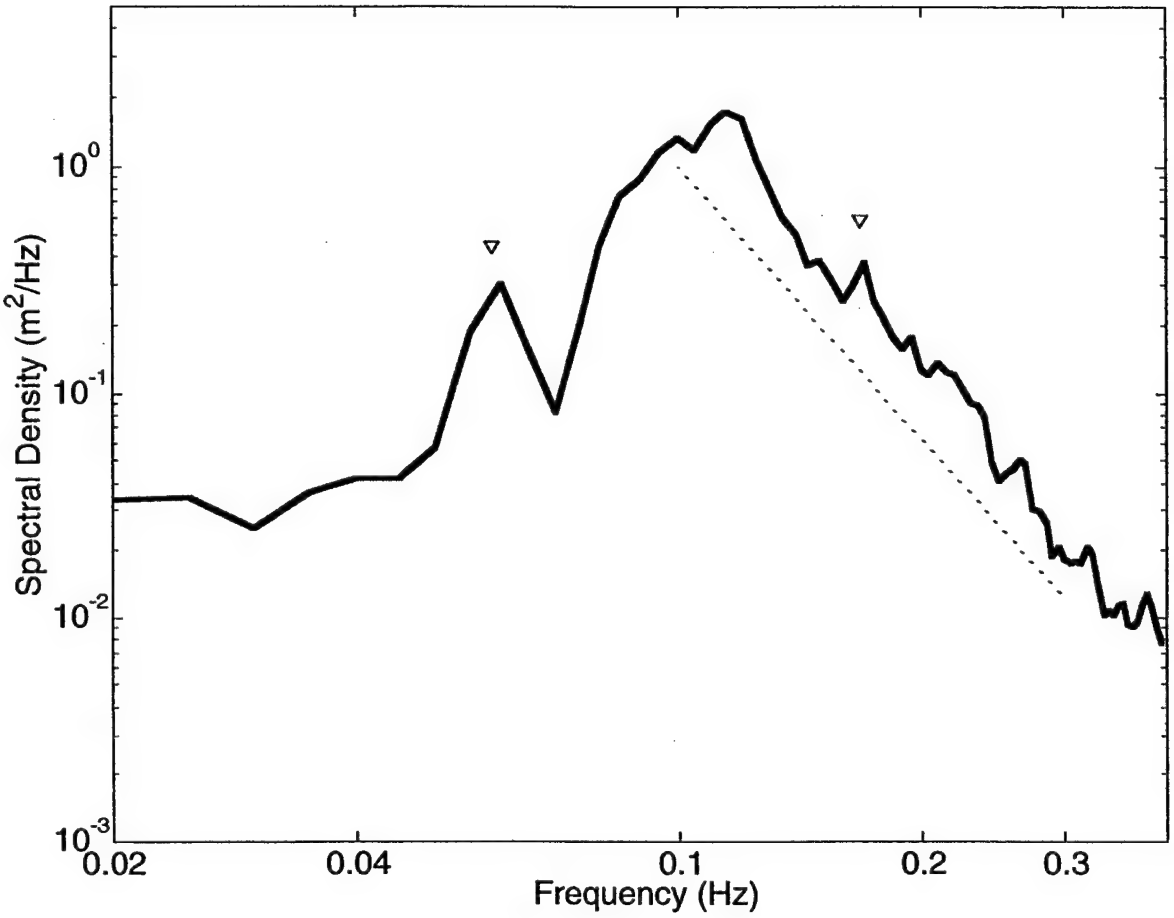
Spectral Density (m²/Hz)
10⁰
10⁻¹
10⁻²
10⁻³
0.02
0.04
0.1
0.2
0.3
Frequency (Hz)

F4

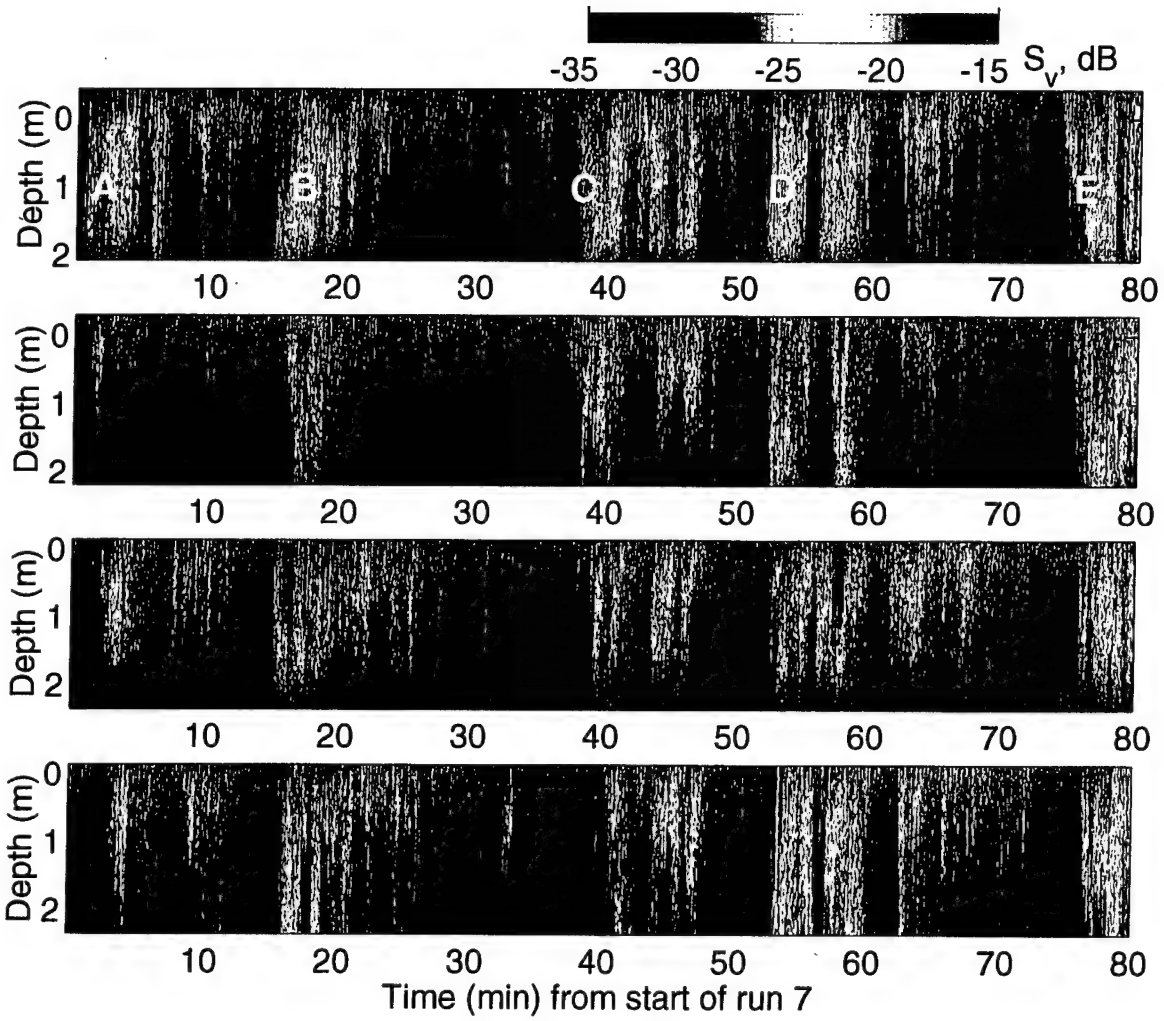
-35 -30 -25 -20 -15 S_v, dB
Depth (m)
0
1
2
A
B
C
D
E
10 20 30 40 50 60 70 80
Time (min) from start of run 7

F5

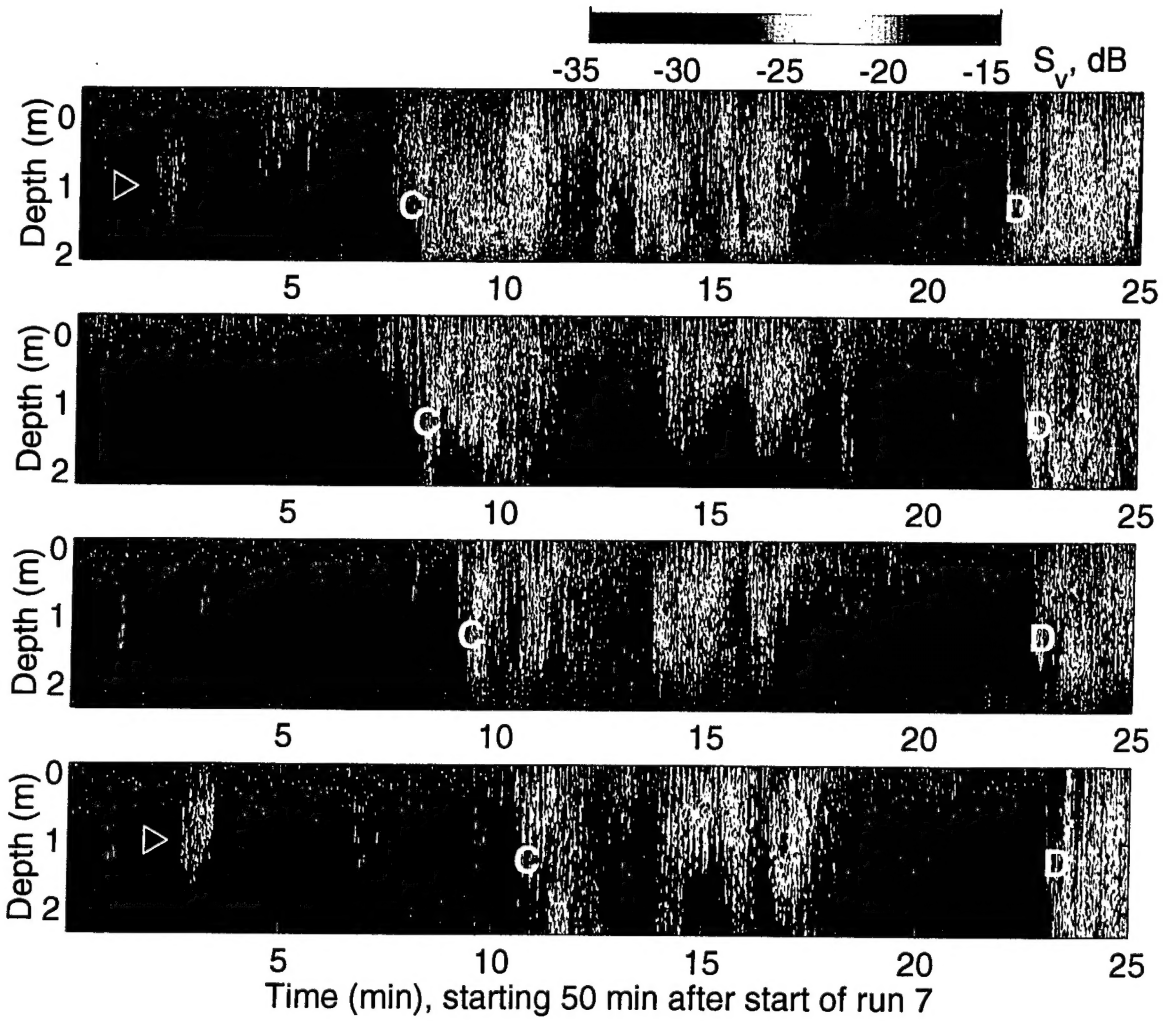
-35 -30 -25 -20 -15 S_v, dB
Depth (m)
0
1
2
C
D
5 10 15 20 25
Time (min), starting 50 min after start of run 7

F6

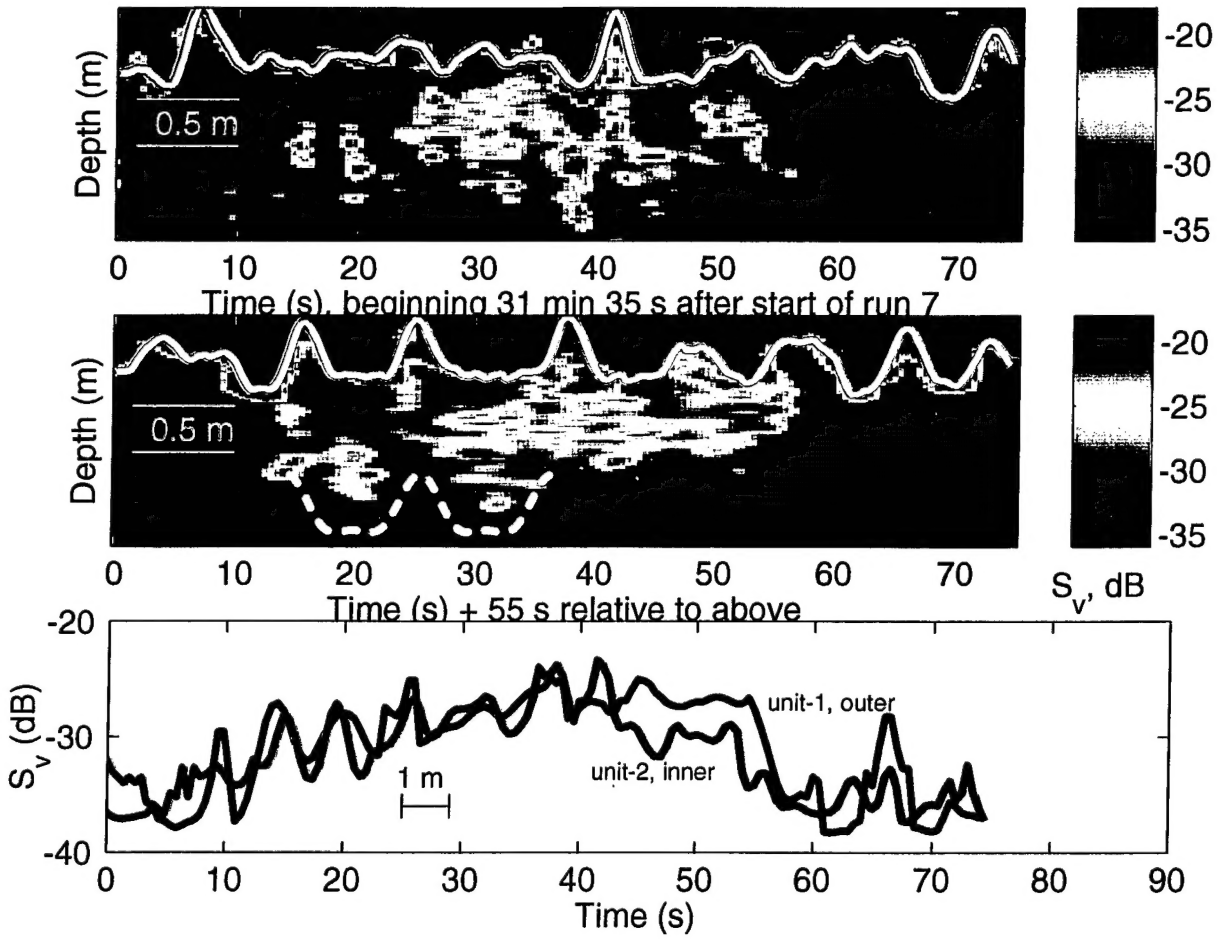
Depth (m)
0.5 m
-20
-25
-30
-35
0
10
20
30
40
50
60
70
Time (s), beginning 31 min 35 s after start of run 7
Depth (m)
0.5 m
-20
-25
-30
-35
0
10
20
30
40
50
60
70
Time (s) + 55 s relative to above
S_v, dB
-20
-30
-40
S_v (dB)
unit-1, outer
unit-2, inner
1 m
0
10
20
30
40
50
60
70
80
90
Time (s)

F7

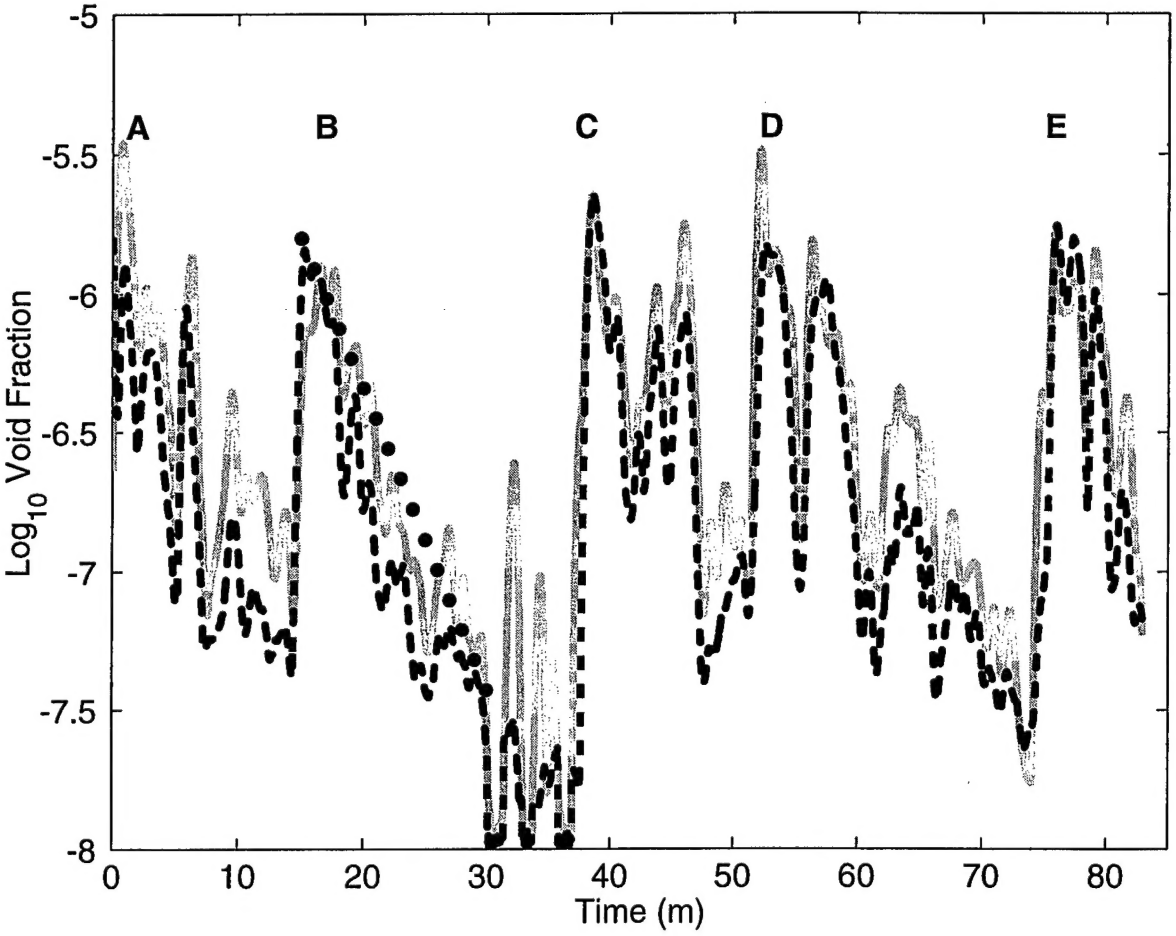
A
B
C
D
E
-5
-5.5
-6
-6.5
-7
-7.5
-8
Log10 Void Fraction
0
10
20
30
40
50
60
70
80
Time (m)

F8

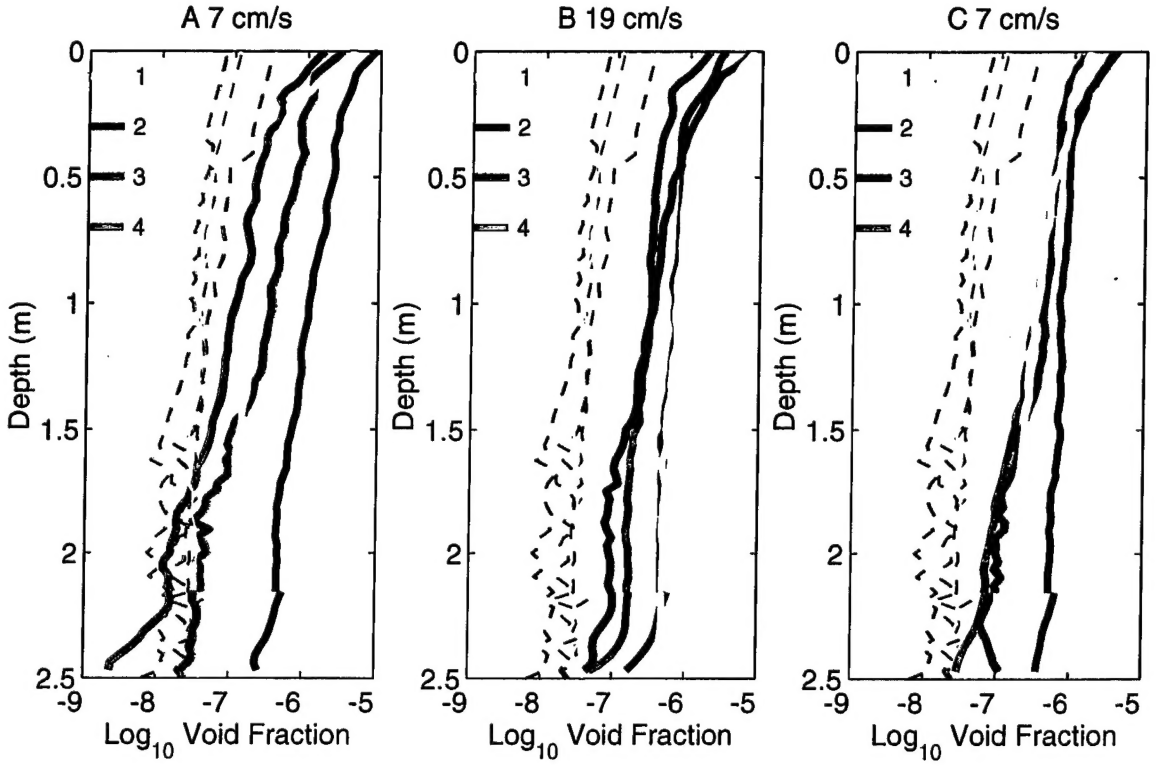
A 7 cm/s
B 19 cm/s
C 7 cm/s
Depth (m)
Log10 Void Fraction
1
2
3
4

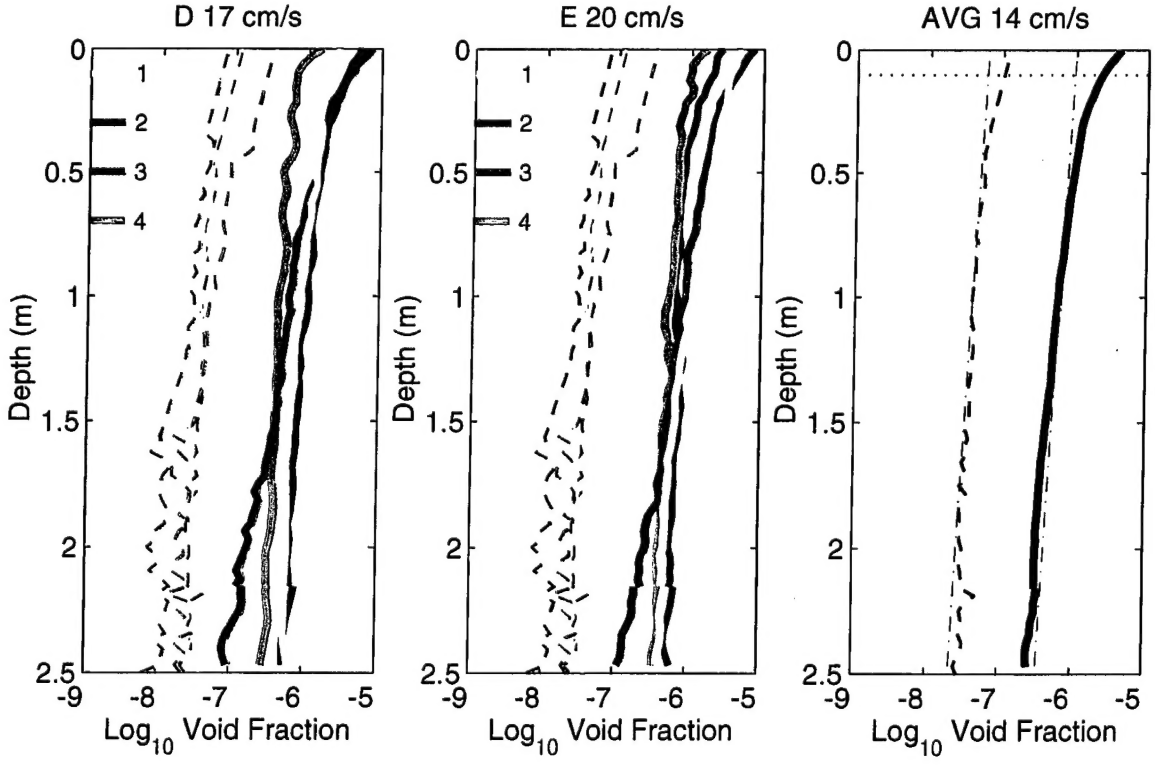
D 17 cm/s
E 20 cm/s
AVG 14 cm/s
Depth (m)
Log10 Void Fraction
1
2
3
4

F9